Reliability Analysis of the Ultrasonic Inspection System for the Inspection of Hollow Railway Axles

Mato PAVLOVIC [1], Christina MÜLLER [1], Thomas HECKEL [1], Andreas ZOËGA [2]
[1] Bundesanstalt für Materialforschung und -prüfung (BAM), Berlin, Germany
[2] DB Systemtechnik GmbH, Brandenburg-Kirchmöser, Germany

Contact e-mail: mato.pavlovic@bam.de

Abstract. Axles are safety critical train components that are subjected to significant cyclic loading during operation. If the crack is initiated in the axle, cyclic loading will lead to crack propagation. To maintain structural integrity, axles must be periodically inspected for fatigue cracks in the material. Deutsche Bahn uses mechanized ultrasonic inspection system to inspect hollow railway axles. The inspections are performed from the bore surface, using several conventional transducers with different incident angles, inspecting the axle along the entire length. As with the every safety critical system, the reliability of these inspections must be determined with regard to their flaw detection capabilities. Traditionally this is done according to the relevant standards for railway vehicles. To investigate the capability of the NDT system more thoroughly, we want to evaluate the capability of the inspection system to detect flaws by means of probability of detection (POD) curves. It will be shown that other parameters, beside the size of the crack, for example crack position in the axle, influence the detection of the crack. The influence of these parameters was evaluated using ultrasonic simulation. The evaluation served as an input for the manufacturing of the flaws in the real scale axle. Once these axles are inspected and the data evaluated, using data from both measurement and simulation, we will express the POD of the crack as function of influencing parameters using the multiparameter POD model.

1. Introduction

Railway axles are safety critical components. If, during operation, a crack is initiated in the axle, it can be assumed that it will propagate under the cyclic loading perpendicular to the axis of the axle [1]. For this reason, axles are periodically checked for flaws by means of NDT By trying to detect ever smaller flaws, NDT systems are pushed to their limits, resulting in inconsistent flaw detection. Some flaws of the same size are detected and some are missed. The same flaw, by repeated inspections, will sometimes be detected, and sometimes not. The capability to detect (small) flaws is therefore expressed as the reliability of the NDT system. The probability of detection (POD) curve is a standard tool to express the reliability of NDT systems. The capability of the automated ultrasonic (UT) inspection system to detect flaws in the hollow railway axles is performed according to the standard DIN 27 201 [2]. A system's acceptability is determined by its ability to detect an artificial flaw (a saw cut) of 2mm depth extension in the axle, with a 6 dB safety margin. However, it has been postulated that these systems can detect much smaller flaws [3]. It has also been shown that saw cuts, as ultrasonic reflectors, are bad representatives of the real

cracks that propagate in axles, for cracks with a depth extension less than 2 mm [3]. For this purpose, a semielliptical planar reflector is a better choice [4]. To assess the reliability of the automated UT inspection system for inspection of hollow axles, we first investigated factors that influence detection using UT simulation. We selected four factors for the investigation: the depth of the semielliptical planar flaw, its position in the axle, the refraction angle of the transverse ultrasonic wave and the delay path. The response variable was the maximum reflected amplitude. We performed a full factorial design. The analysis of the results showed that the depth extension of the flaw and its position are essential influencing factors. This output will serve as an input for the production of the Electrical Discharge Machining (EDM) semielliptical notches in the test axles. Once the notches have been manufactured, the axles will be inspected by the UT system. Using the measured data and the results of simulation, we will assess the reliability of the system with the multiparameter POD model [5]. The final goal is to assess the UT system reliability on the real fatigue cracks. This paper presents our progress towards this goal. In the first section of the paper, a brief description of reliability of NDT is given. It is followed by the description of the mechanised UT system used for the inspection of hollow railway axles. In the third section, the UT simulation of one of the transducers in the system is described. The results of variation of four factors across all levels are presented and discussed in the fifth section. Finally, conclusions and an outlook are given in the last section.

2. Reliability of NDT

When pushed to their limits, by attempting to detect small flaws, NDT system indications are inconsistent. Therefore, in applications where a missed flaw can have catastrophic consequences, the reliability of the NDT system has to be established. The POD curve is considered to be a standard tool to quantify the reliability of NDT [6]. A signal response model [7] assumes that the response signal is correlated with the flaw size. The POD and a lower 95% confidence bend are calculated. The $a_{90/95}$ point determines the limit of reliable use of the NDT system. When there are more factors that influence the POD of the flaw, the signal response model is not applicable any more. The multiparameter model, on the other hand, allows several parameters to be included in the analysis and enables the POD to be expressed as a function of these.

3. Mechanised Ultrasonic System for the Inspection of Hollow Train Axles

Hollow railway axles are inspected from the bore surface. A typical configuration of such system is shown in Fig. 1. The ultrasonic transducers are located in the probe module. The system is docked to the side of the axle and the probe module is pushed into the borehole. The feed mechanism moves the probe module in the axial direction and at the same time it rotates around the axis, so that transducers describe a helical path. The feeding mechanism also delivers coupling oil to the probe module and transfers the signals from the transducers to the control unit. Several transducers with different angles of incidence are mounted in the probe head with the aim of detecting cracks on the outer surface of the axle.

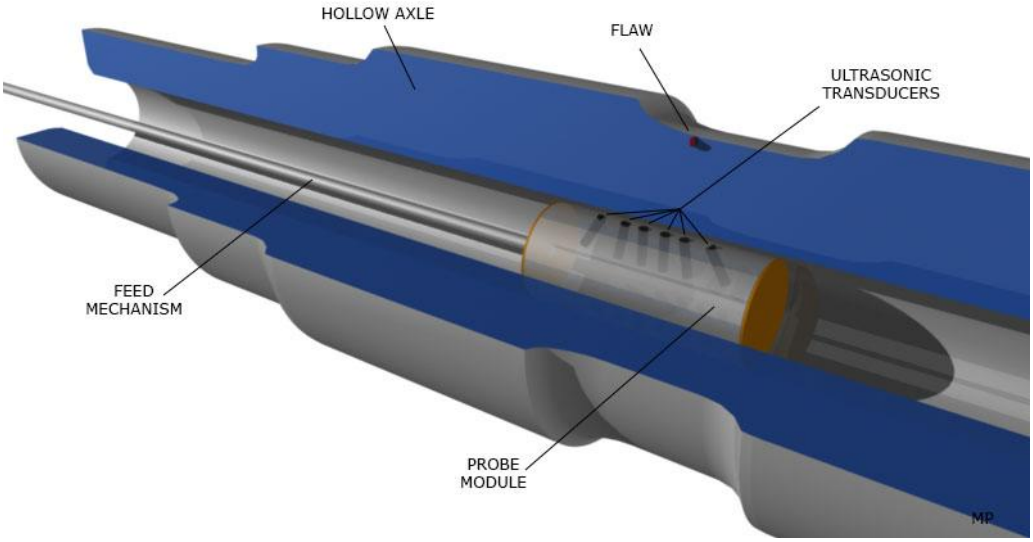

Fig. 1. Cross section of the hollow axle with a probe module in the borehole.

The detection of the planar, surface breaking flaws that are perpendicular to the surface is mainly based on the corner reflection effect. The ultrasonic wave that hits the back surface of the inspected component under a favourable angle is reflected to the flaw and then back to the transducer. Since the outer surface of the axle has a variable diameter, the cracks which propagate perpendicular to the axis of the axle shortly after initiation, will have 90° angle to the surface only in the regions of the axle where the diameter is constant. The angle between the flaw and the surface will have an influence on the corner reflection effect and therefore also on the detectability of the flaw. The transition region between the wheel seat and the body of the axle is considered as particularly susceptible to cracking. This is where we concentrated our investigations.

4. Ultrasonic simulation

In order to establish which factors play a major role in detection and the extent of their influence thereon, we concentrated our investigation first on one of the transducers in the probe module. The transducer we investigated is a circular transducer with an 8 mm diameter and a 5 MHz centre frequency, which is mounted in the probe module so that it generates 35° transverse wave in the axle. To properly address the influence of the geometry on the reflected amplitude, we modelled the exact geometry of the axle with a CAD software. The geometry was imported in the UT simulation software, together with the flaw and transducer definitions. The simulation was performed with CIVA 2015 (11.1).

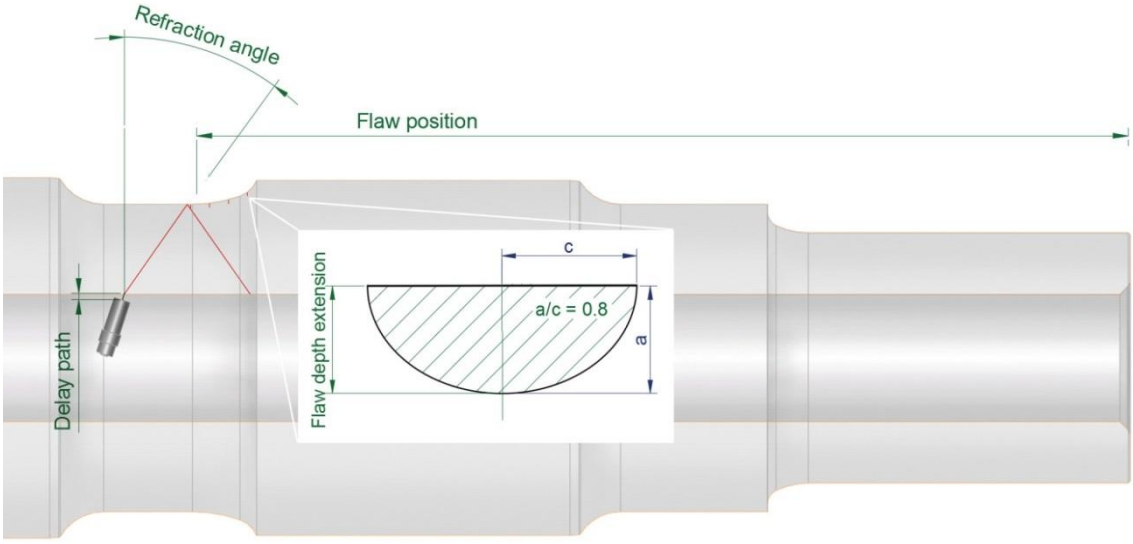

Fig. 2. Parameters selected for the investigation.

Four parameters have been chosen for the investigation: flaw position, flaw depth extension, delay path and reflection angle. The parameters are illustrated in Fig. 2. The angle between the flaw and the outer surface, which has a direct influence on the corner reflection effect, is determined by the location of the flaw. The position of the flaw is chosen to be in the transition region between the wheel seat and the body of the axle. The type of the flaw used in the investigation is a semielliptical planar flaw with an aspect ratio of minor and major axes of 0.8. The flaw is also illustrated in Fig. 2. The flaw depth extension is varied, while maintaing the minor/major axes ratio of 0.8. The third parameter we investigated was the delay path. The coupling oil, provided by the probe module via the feeding mechanism, ensures that the transducers are working in the immersion mode. We wanted to find out the influence of the transducers' distance to the bore surface on the reflected amplitude. Finally, the refraction angle of the transverse wave is chosen as a fourth parameter. Since transducers with different angles are used in the probe head to ensure the detection of all flaws, we wanted to investigate the influence of the refraction angle on the reflection amplitude. The levels of all factors are given in Table 1. The maximum amplitude was calculated by varying all factors across all levels, performing a full factorial design.

Table 1. Factors with levels used in UT simulation

Delay Path [mm]	1	3	5	
Refraction Angle [°]	-40	-35		
Flaw Position [mm]	495	485	475	465
Flaw Depth Extension [mm]	0.5	1.0	1.5	2.0

5. Results and Discussion

First we calculated the sound field that the transducer generates in the axle. An axial cross section of the sound field is shown in Fig. 3. The magnitude of the amplitude along the central axis of the beam (indicated with a red line in Fig. 3) is shown in Fig.4.

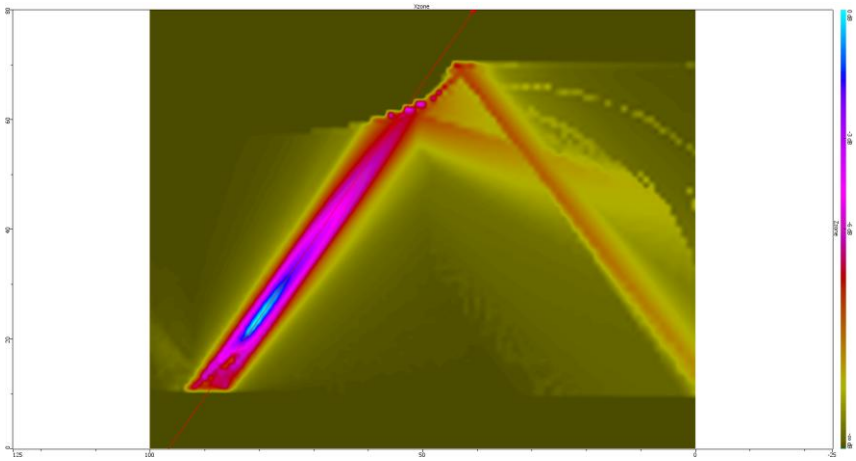

Fig. 3. An axial cross section of the sound field, with the centre axis of the field indicated with a red line.

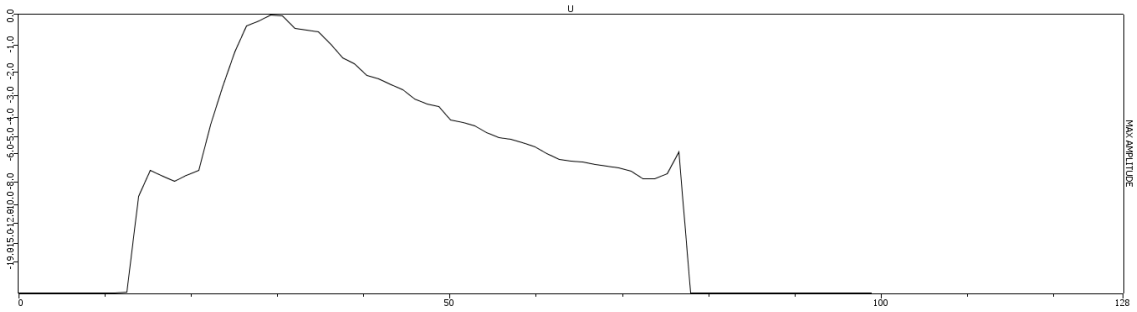

Fig. 4. Amplitude change along the centre axis of the sound field

This is the line of maximum amplitude and it is, as expected, inclined by 35°. It can be observed how the amplitude increases with the distance from the transducer, then reaches its maximum and declines thereafter. An additional effect caused by the curvature of the inspection surface (i.e. the borehole of the axle) can be seen in the radial cross section. The geometry of the axle acts as a lens and focuses the beam. In Fig. 5a, the beam of rays is shown in radial cross section, where this effect is clearly visible. Fig. 5b and Fig. 5c show the radial cross section of the sound field at the inner and at the outer surface of the axle, respectively. Since the change of the sound field as the wave propagates is influenced by the focusing effect, the reflected amplitude will also be affected by the distance of the flaw from the transducer. This is again correlated with the geometry of the axle.

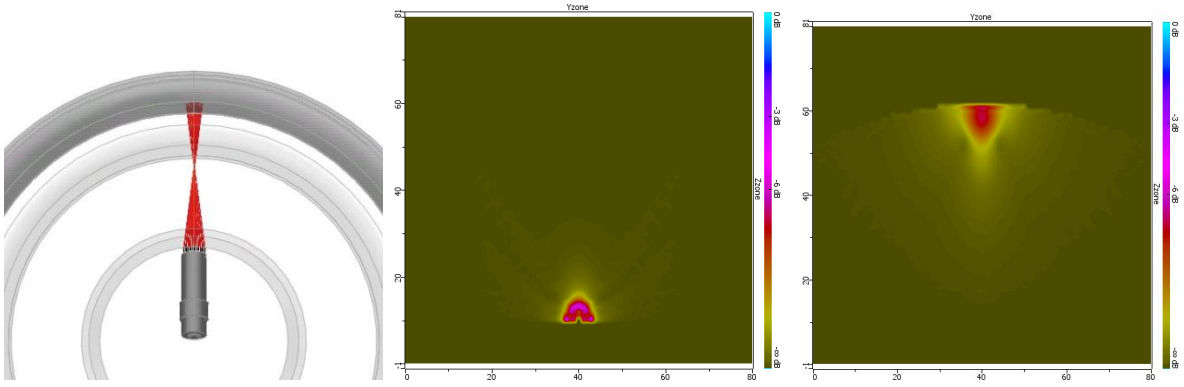

(a) (b) (c)

Fig. 5. The beam of rays focusing caused by the curvature of the axle (a).

A radial cross section of the sound field at the inner (b) and outer surface (c).

The change of the maximum amplitude with a position of the flaw, for three different delay paths, is shown in Fig. 6. It can be observed that the amplitude changes depending on the position of the flaw. Reflected amplitude is higher for the flaws located at the positions 495 and 485 mm than for the flaws at positions 475 and 465 mm. Furthermore, the delay path of 1 mm results in smaller amplitudes than the delay paths of 3 and 5 mm, for all positions of the flaw. However, this difference is very small.

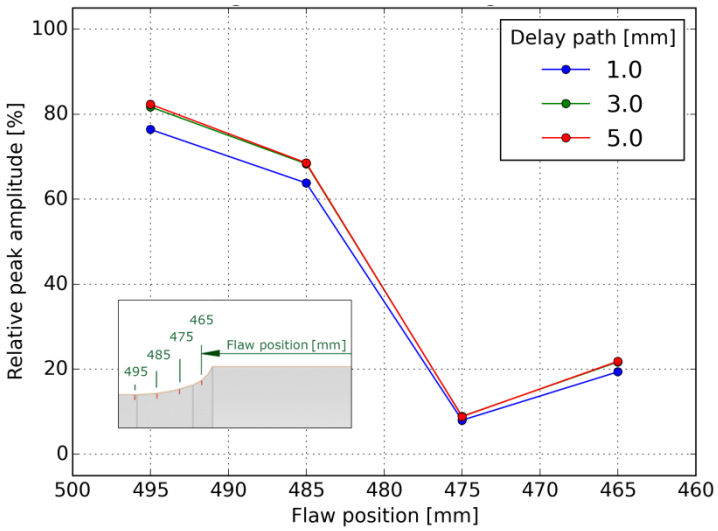

Fig. 6. Calculated relative peak amplitude as function of the flaw position, for different delay paths. Refraction angle is -35°, flaw depth extension 2.0 mm.

In Fig. 7, the change of the amplitude is shown as a function of flaw position, for two refraction angles. Flaws at the position 495 and 485 mm have larger amplitudes than the flaws at positions 475 and 465 mm.

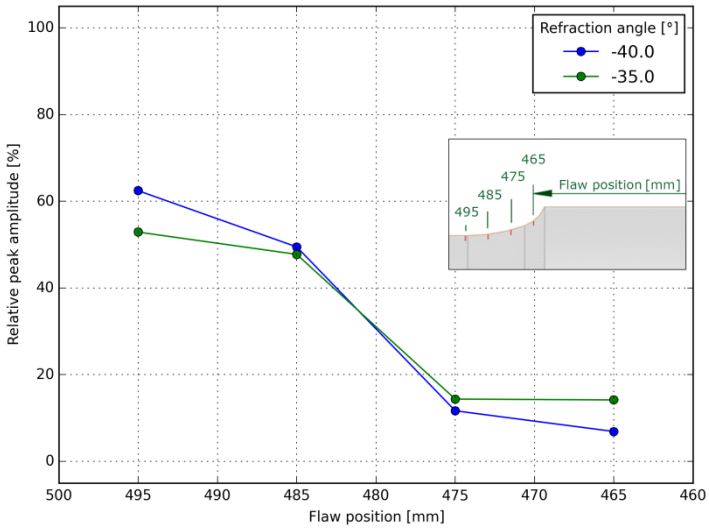

Fig. 7. Calculated relative peak amplitude as function of the flaw position, for different refraction angles. Delay path is 3 mm, flaw depth extension 1.5 mm.

Finally, Fig. 8 shows the change of the reflected maximum amplitude with the position of the flaw for four different flaw depth extensions. Again it can be observed that amplitudes

vary, depending on the position of the flaw. Flaws at the position 495 and 485 mm have higher amplitudes than the flaws of the same depth extension at positions 475 and 465 mm, regardless of their size. Also, as expected, the bigger is the flaw, the higher is the reflected amplitude, regardless of the flaw position. The only exception was the 2.0 mm flaw at the position 475 mm. This could just be a strange anomaly, but it seems worthy of further investigation.

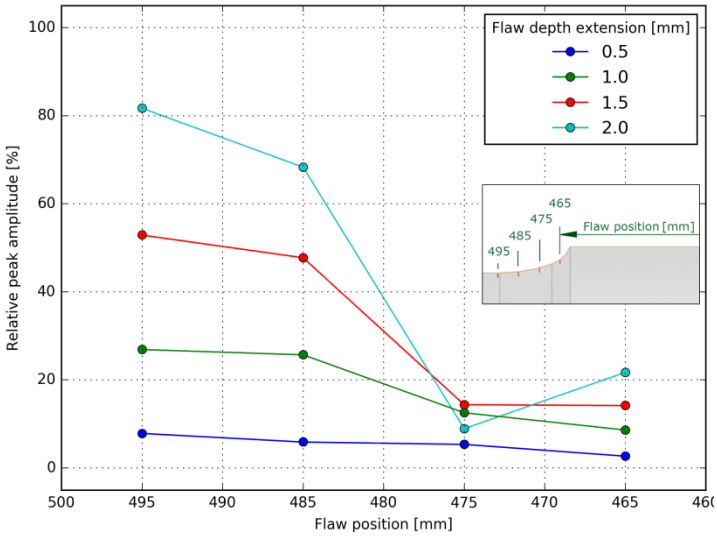

Fig. 8. Calculated relative peak amplitude as a function of the flaw position, for different flaw depth extensions. Delay path is 3 mm and refraction angle is -35°.

To this end we first analysed the amplitudes of the 1.5 mm flaw at the positions 475 and 465 mm (red line in Fig. 8). They are almost of the same magnitude, although the flaws are at different positions. For deeper analysis, we used a feature of CIVA that enables tracking of the wave from the transducer over the reflections that occur in the component on its path back to the transducer. The composition of the amplitude measured by the transducer is decomposed into the contributions of individual waves. The beam of rays illustrating the reflections of the wave on the outer surface of the axle and the flaw are shown in Fig. 9. The amplitude of the flaw at the position 475 mm is composed in the following way: 38.2% flaw-surface, 35.8% surface-flaw, 16.5% surface-flaw-surface and 9.5% is the direct reflection from the flaw. The amplitude of the flaw at the position 465 mm is on the other hand, composed in the following way: 69.7% surface-flaw-surface, 10.6% flaw, 10.2% flaw-surface and 9.6% surface-flaw. For the flaw at position 475 mm, the major part of the reflected amplitude comes from the corner reflection effect (38.2+35.8=74%). On the other hand, the majority of the reflected amplitude (69.7%) of the flaw at the position 465 mm comes from the double reflection surface-flaw-surface. So even if we measure the same amplitude for both flaws, the origin of this amplitude is quite different. We could explain the lower amplitude of the 2.0 mm flaw than from the smaller flaws at the position 475 mm in the same way. Due to the larger size of the flaw, several reflections of the sound wave occur between the flaw and the surface, so only small part of the wave is reflected back to the transducer.

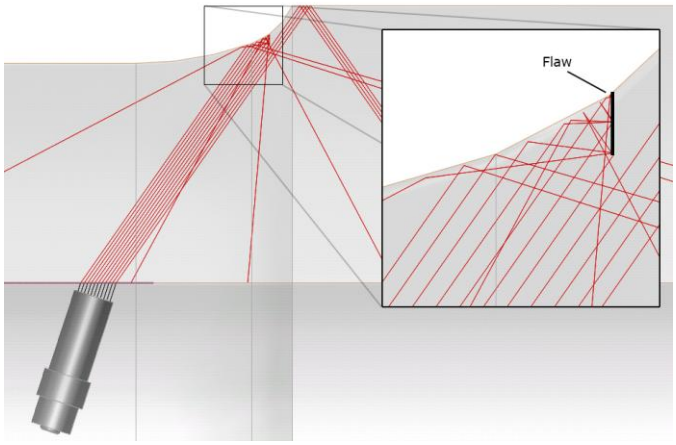

Fig. 9. Multiple reflections of the wave on the outer surface of the axle and the flaw.

6. Conclusions and Outlook

The results show that all investigated parameters have an influence on the reflected amplitude and will therefore influence the POD of the flaw. The two most important parameters, the depth extension and the position of the flaw, have been identified. Based on these results, the manufacturing of the EDM flaws with varying depth extension and position will be carried out in the real size axles. The axles will be then inspected with the UT system and the UT data will be evaluated. The investigation presented in this paper concentrated only on one transducer. The simulation will be performed for all transducers in the UT system used for the detection of circumferential flaws on the outer surface of the axle. Once both the theoretical amplitudes from simulation and the amplitudes measured by the UT system are available, the POD will be calculated using the multiparameter POD model. Since the model determines the POD of individual transducers, a data fusion process will be necessary to determine the overall POD of the whole UT system.

7. References

[1] Zerbst U., Vormwald M., Andersch C., Mädler K., Pfuff M., The development of a damage tolerance concept for railway components and its demonstration for a railway axle, Engineering Fracture Mechanics, Volume 72, Issue 2, January 2005, Pages 209-239, ISSN 0013-7944, http://dx.doi.org/10.1016/j.engfracmech.2003.11.011.

[2] DIN 27201-7 :2014-05, State of railway vehicles – Basic principles and production technology – Part 7: Non-destructive testing, Beuth, 2014.

[3] Zoëga A., Hintze H., Rohrschneider A., Kurz J., Pavlovic M., Kanzler D., Müller C., "Investigations to Introduce the Probability of Detection Method for Ultrasonic Inspection of Hollow Axles at Deutsche Bahn", Proceedings 19th World Conference on Non-Destructive Testing, 2016.

[4] Zerbst U., Mädler M., Hintze H., Fracture mechanics in railway applications—an overview, Engineering Fracture Mechanics, Volume 72, Issue 2, January 2005, Pages 163-194, ISSN 0013-7944, http://dx.doi.org/10.1016/j.engfracmech.2003.11.010.

[5] Pavlovic M, K Takahashi and C Müller. 2012. "Probability of Detection as a Function of Multiple Influencing Parameters." Insight 54(11):606-611.

[6] Rummel W.D., Probability of Detection As a Quantitative Measure of Nondestructive Testing End-To-End Process Capabilities. Materials Evaluation, 56, 1998.

[7] Berens A.P., "NDE Reliability Data Analysis." ASM Metals Handbook, Volume 17, 9th Edition: Nondestructive Evaluation and Quality Control. ASM International, Materials Park, Ohio, pp. 689-701. 1988.